Published in final edited form as:

Structure. 2008 November 12; 16(11): 1732–1739. doi:10.1016/j.str.2008.08.017.

Structure of the Kinesin13-Microtubule Ring Complex

Dongyan Tan[1], **William J. Rice**[2], and **Hernando Sosa**[1,*]

[1]Department of Physiology and Biophysics, Albert Einstein College of Medicine, Bronx NY, 10461, USA

[2]New York Structural Biology Center, New York, NY 10027, USA

SUMMARY

To investigate the mechanism of kinesin13-induced microtubule depolymerization, we have calculated a three-dimensional (3D) map of the kinesin13-microtubule ring complex, using cryo-electron microscopy (cryo-EM) and image analysis. An atomic model of the complex was produced by docking the crystal structures of tubulin and a kinesin13 motor domain (MD) into the 3D map. The model reveals a snapshot of the depolymerization mechanism by providing a 3D view of the complex formed between the kinesin13 MD and a curved tubulin protofilament (pf). It suggests that contacts mediated by kinesin13 class-specific residues in the putative microtubule-binding site stabilize intra-dimer tubulin curvature. In addition, a tubulin-binding site on the kinesin13 MD was identified. Mutations at this class-conserved site selectively disrupt the formation of microtubule-associated ring complexes.

INTRODUCTION

All members of the kinesin superfamily of microtubule-associated motor proteins convert the energy from ATP hydrolysis into mechanical work. The defining element of the superfamily is the presence of a highly conserved (~320 residues) catalytic or motor domain (MD) that contains the ATP and microtubule-binding sites (Goldstein and Philp, 1999). Most kinesins pull cargoes along microtubules, but an important exception is found in the kinesin13 family, also known as Kin-Is or M kinesins (because of the central location of the MD in the polypeptide chain). Instead of walking along microtubules, kinesin13s promote the disassembly of microtubule ends (Desai et al., 1999), an activity that is important for modulating microtubule dynamics during mitosis (Ganem and Compton, 2004; Rogers et al., 2004) and interphase (Mennella et al., 2005). Kinesin13 activity has been shown to be necessary for proper development of the nervous system (Homma et al., 2003), and its overexpression is associated with some forms of cancer (Ishikawa et al., 2008; Ovechkina and Wordeman, 2003).

*Correspondence: hsosa@aecom.yu.edu.

ACCESSION NUMBERS The electron density map has been deposited in the EM Data Bank (EMDB) under accession number EMD-5027, and the atomic model of the complex has been deposited in the Protein Data Bank under PDB code 3EDL.

SUPPLEMENTAL DATA Supplemental Data include two figures and can be found with this article online at http://www.structure.org/cgi/content/full/16/11/1732/DC1/.

The kinesin13-induced depolymerization mechanism most likely involves the bending of protofilaments (pfs) at the end of the microtubule (Wordeman, 2005). The bent pfs, which are unable to form lateral contacts, peel off from the microtubule and ultimately cause depolymerization. The kinesin13 MD alone binds to curved tubulin pfs and is sufficient to induce microtubule depolymerization (Moores et al., 2002). A region N-terminal to the MD (~30 residues) called the neck increases depolymerization efficiency (Maney et al., 2001). The physical mechanism by which kinesin13 stabilizes tubulin curvature is unclear. It is also unclear how the highly conserved kinesin MD is adapted in different families, for either walking along or bending tubulin.

Constructs containing the kinesin13 MD form oligomeric rings and spirals around microtubules in vitro in the presence of the nonhydrolyzable ATP analog AMP-PNP (Moores et al., 2006; Tan et al., 2006). No other kinesins have been reported to form such rings. Whether the formation of these oligomers is important for the depolymerization mechanism or some other kinesin13 functionality is still not clear (Davis and Wordeman, 2007; Tan et al., 2006). Image analysis of negatively stained kinesin13-microtubule ring specimens indicated that part of the ring structure was formed by kinesin13 MDs interacting with a curved tubulin pf (Tan et al., 2006). Thus, these rings/spirals provide a snapshot of the mechanism of kinesin13-induced tubulin curvature. Here, we have used cryo-electron microscopy, 3D reconstruction, and molecular docking to produce an atomic model of the kinesin13-microtubule ring complex. We then tested the effect, on kinesin13 function, of mutations on residues predicted by the model to from intermolecular contacts. We found a novel microtubule-binding site on the MD that is conserved in the kinesin13 family. The presence of this conserved binding site suggests that the interactions leading to the formation of rings and spirals are relevant to kinesin13 function.

RESULTS

Ring Formation Is Conserved within the Kinesin13 Family

We previously found that constructs containing the MD of three different kinesin13s from two animal species, *Drosophila melanogaster* KLP10A and KLP59C and *Cricetulus griseus* (Chinese hamster) MCAK, all form rings around MTs in vitro in the presence of AMP-PNP or ATPγS(Tan et al., 2006). To further investigate the generality of this ring-forming ability within the kinesin13 family, we extended our studies to two human kinesin13s. After incubating MD constructs of human KIF2A and KIF2C with microtubules in the presence of AMP-PNP, we observed rings and spirals on microtubules very similar to those formed by other kinesin13s (Figure 1).

These results indicate that the ability to form microtubule-associated rings is conserved within the kinesin13 family. Only the MD is required to form the rings, so class-conserved residues (present in the kinesin13 family but different in other kinesins that do not form rings) in the MD must mediate the interactions leading to ring formation. To determine candidate residues mediating the formation of the rings, we built an atomic model of the ring/spiral complex based on cryo-EM imaging, followed by molecular docking.

Structure of the KLP10A-Microtubule Ring Complex

Very regular spirals, suitable for 3D reconstruction, form when incubating KLP10A MD constructs with microtubules in the presence of AMP-PNP. For structural analysis, we selected microtubules with 15 pfs that have no lattice seams (Sosa and Milligan, 1996). Previously we obtained a 3D reconstruction from a negatively stained specimen that allowed us to propose a molecular model of the kinesin13-microtubule ring complex (Tan et al., 2006). However, we noted that in the previous map, densities near the microtubule were not well fit by the docked atomic structures (Tan et al., 2006). To avoid potential staining artifacts and to improve the resolution, we have now analyzed frozen-hydrated kinesin13-microtubule ring complexes by cryo-EM. Cryo-EM produces electron density maps that are derived directly from the molecular structure of the specimen (not from a heavy metal cast) and are less prone to flattening artifacts.

Figures 2A and 2B show a cryo-electron micrograph of a KLP10A MD-microtubule complex and the corresponding power spectrum. The spacing of the layer lines in the power spectrum corresponds to a 15-pf microtubule lattice. The absence of layer lines with a different spacing indicates that the KLP10A MD complex spiral follows the tubulin lattice, consistent with our previous structural analysis of negatively stained specimens (Tan et al., 2006). We observed clear layer lines in the power spectrum of individual images to a resolution of 2.7 nm (Figure 2b). A surface representation of a 3D map calculated by helical reconstruction from several frozen-hydrated filaments is shown in Figure 2c. The resolution of the map was estimated at 2.8 nm by the Fourier Shell Correlation (FSC) 0.5 cutoff criteria (Frank, 2002), signal above noise extended to a resolution of 1.5 nm (see Figure S1 available online). A distinctive feature of the 3D map is the continuous spiral of densities at the outermost radius following the two start left-handed helical path of the tubulin lattice. This feature was also present in the previous negative staining 3D map.

There are some differences between the previous negative stain map and the current cryo-EM map. The most significant are the presence of extra density closer to what would be the microtubule and a slightly larger separation between the densities corresponding to the microtubule and the outer ring (Figure 2d). The differences between the current and previous maps could be due to staining artifacts or to the presence of extra proteins in some filaments. It is plausible that the rings may, on occasion, encircle some KLP10A MDs already bound to the microtubule lattice, giving rise to extra density closer to the microtubule wall. However, inspection of the separation between the microtubule and the outside ring (Figure 2d) in many filaments revealed a correlation with the preparation method (cryo: 9.43 ± 0.08 nm, $n = 94$, neg.-stain: 10.17 ± 0.15 $n = 80$, mean ± SE, $p << 0.01$), suggesting the presence of staining artifacts and/or flattening in the reconstruction from negatively stained samples. A major consequence of the differences between the maps is that only one kinesin MD per asymmetric unit fits in the cryo-EM map densities. The new cryo-EM map also produces a better fit overall after docking of the atomic structures (see below).

Molecular Model of the Kinesin13-Microtubule Ring Complex

An atomic model of the ring complex was obtained by fitting (docking) the atomic structures of the tubulin and a kinesin13 MD into the electron density map (Figure 3). Fitting was done

quantitatively using the program COLORES (Chacon and Wriggers, 2002). Two tubulin heterodimers and one kinesin MD were fitted into the asymmetric unit of the complex. A straight tubulin heterodimer fits into the innermost density of the complex, forming the microtubule scaffold, whereas a second curved tubulin heterodimer fits into the outermost region of the ring forming an isolated curved pf. In this model, the exterior face of this second tubulin heterodimer corresponds to the face that is normally exposed to the luminal side of the microtubule. We found that antibodies directed against the luminal side of tubulin label the outside of the ring (Figure S2), providing independent support for this fitted orientation. The two tubulin heterodimers are oriented approximately perpendicular to each other, and both form intermolecular contacts with the kinesin MD, which is sandwiched in between. The relative configuration between the kinesin MD and the outer tubulin heterodimer is similar to the orientation found in other kinesin-microtubule complexes, indicating a similar binding interface (Figure 4). This configuration is also consistent with projected views of kinesin13s bound to isolated pf rings (Moores et al., 2002). We will call the interface between the kinesin MD and the curved tubulin in the outside ring “Kin-Tub-1,” and the interface between the MD and the inner tubulin in the microtubule “Kin-Tub-2” (Figure 3C).

The densities in the cryo-EM map corresponding to the tubulin subunits in the outside ring have slightly different intra- and inter-dimer radial curvature angles (11° and 13°)(Figure 3D). We identified one α-β tubulin heterodimer as the two tubulin subunits contacting the kinesin MD, on the basis of the similarity of the Kin-Tub-1 interface with other kinesin-tubulin complexes (Marx et al., 2006). Accordingly, the smallest radial curvature angle between tubulins in the curved pf (11°) corresponds to the intra-dimer interface, and the tip of the kinesin13 KVD-loop is closer to α-tubulin (Figures 3D and 4).

Previous studies have shown that mutations at the KVD loop and α-helix-4 strongly reduce depolymerization activity (Ogawa et al., 2004; Shipley et al., 2004), indicating that kinesin residues near the Kin-Tub-1 interface are important for depolymerization. Further insights into the mechanism of depolymerization are provided by comparing the Kin-Tub-1 interface and the kinesin1-microtubule complex (Figure 4). A major difference between these two complexes is the presence of the elongated class-specific KVD loop in kinesin13s, extending toward α-tubulin and contacting it when the tubulin heterodimer is in the curved configuration (Figure 4). Thus, the model supports a mechanism for kinesin13-induced microtubule depolymerization in which interactions between the KVD loop and α-tubulin, together with the other interacting sites at the Kin-Tub-1 interface (kinesin α-helix-4 with the tubulin intra-dimer interface and kinesin loops 8 and 12 with β-tubulin), stabilize tubulin intra-dimer curvature (Figure 4).

It has also been proposed that direct interactions between the KVD-loop and the tubulin inter-dimer interface stabilize inter-dimer curvature (Ogawa et al., 2004). However, in our model, the KVD loop is not close enough to the β-tubulin in the next heterodimer along the pf to make direct contacts. Therefore, our model does not suggest a direct effect of the kinesin13 MD on tubulin inter-dimer curvature. It is possible that kinesin13 binding does not stabilize a kinked tubulin inter-dimer curvature directly. Instead, a bent inter-dimer interface

could be the stable configuration, when a tubulin pf is outside the microtubule wall without inter-pf lateral contacts (Rice et al., 2008).

The interface Kin-Tub-2 is a novel kinesin tubulin-binding site not previously described. Analysis of the amino acid sequence in this area reveals several class-specific residues (Figure 5) for the kinesin13 family, suggesting that interactions at the Kin-Tub-2 interface are important for kinesin13 function. Of particular interest are several positively charged residues that may form electrostatic interaction with negatively charged residues on the microtubule lattice wall. Our molecular model suggests that both kinesin13-tubulin interfaces are important to form the ring/spiral complex. The Kin-Tub-1 interface is necessary to stabilize pf curvature, and the Kin-Tub-2 interface is necessary to bind the curved pf to the microtubule wall.

Site-Directed Mutagenesis of the Kinesin13-Tubulin Interfaces

To explore the roles of the Kin-Tub-1 and Kin-Tub-2 interfaces on kinesin13 function, we performed site-directed mutagenesis of residues at both interfaces using KLP10A MD constructs. We then tested the constructs for microtubule depolymerization activity and the ability to form rings. We mutated to alanines the sequences KEC and KVD located at the Kin-Tub-1 interface and the residues K399 and K350 located at the Kin-Tub-2 interface (Figure 5). Depolymerization was tested by turbidity at a given concentration of microtubules and kinesin13 MD constructs (see Experimental Procedures). Ring formation was assayed by negative staining electron microscopy of microtubules incubated with each of the constructs in the presence of AMP-PNP. Many microtubules were imaged for each construct and were scored for the presence or absence of rings.

Mutations at the class-specific sequences KEC and KVD, located in the MD α-helix-4 and loop-2, respectively, have already been shown in other kinesin13s to impair microtubule depolymerization activity (Ogawa et al., 2004; Shipley et al., 2004), and we confirmed this finding here with KLP10A. Mutations at these residues reduce the depolymerization activity to 10% or less relative to wild-type (Figure 6). In addition, these mutants are much less likely to form rings/spirals on the microtubules. Compared with wild-type, rings formed on only 0.3% of the microtubules for the KVD mutant and 7.9% for the KEC mutant (Figure 6).

Mutations at the Kin-Tub-2 interface have a distinct effect from the ones at the Kin-Tub-1 interface. The mutants K399A and K350A had depolymerization activity (about 30% higher than wild-type, $p << 0.001$) and severely impaired ability to form microtubule-associated rings. Less than 10% of the microtubules have rings around them, as opposed to 60% for the wild-type construct (Figure 6). However, these mutant constructs induce the formation of many isolated rings, as seen in the background of the images, and individual MDs (not forming rings) can also decorate the microtubule wall (Figures 6D and 6E). These results show that Kin-Tub-2 interactions are necessary for association of the rings to the microtubule but not for depolymerization activity. The slight increase in depolymerization activity over wild-type in these mutants can be readily explained if, in the wild-type constructs, depolymerization is slowed down by the formation of rings at the end of the microtubule. These microtubule-associated rings would hold together the pfs at the end of the microtubule, decreasing the rate of pf peeling.

In summary, the mutagenesis results show that the formation of microtubule-associated rings requires both Kin-Tub-1 and Kin-Tub-2 interactions, whereas depolymerization requires only Kin-Tub-1. The ability to use mutagenesis to separate depolymerization and ring formation will be very useful to test possible roles of ring oligomerization in vivo.

DISCUSSION

We have presented an atomic model of the kinesin13-microtubule ring complex by docking the atomic structures of the kinesin13 MD and tubulin into a cryo-EM map of the complex. The model reveals a 3D snapshot of the complex formed by a kinesin13 MD and a curved tubulin pf. This complex is likely an intermediate state for the kinesin13-induced microtubule depolymerization cycle. The configuration of the kinesin13 MD relative to the curved tubulin observed is very similar to the one seen in other kinesin microtubule complexes (Hirose et al., 2006; Kikkawa and Hirokawa, 2006; Sindelar and Downing, 2007; Sosa et al., 1997). However, class-specific residues at the kinesin-tubulin interface, in particular the extended loop-2 containing the KVD sequence, allow the kinesin13 MD to make new contacts with α-tubulin. These contacts stabilize intra-dimer tubulin curvature that causes the pfs to peel away from the microtubule. This model is consistent with previous studies (Ogawa et al., 2004; Shipley et al., 2004) as well as our current results showing that mutations in the KVD loop severely reduce depolymerization activity.

In addition to the stabilization of curvature in the tubulin heterodimer, our model also reveals a new binding interface between kinesin and tubulin. This is the interface between the kinesin13 MD and the microtubule (Kin-Tub-2, Figure 3). We showed that class conserved residues in this area are critical to ring formation. Some kinesin13s have substitutions in these otherwise class-conserved residues (Figure 5), and our model predicts that these kinesin13s would not have the ability to form microtubule associated rings. Examples of these kinesin13s are *Plasmodium* pKinI, *Drosophila* KLP59D and human KIF2B. In fact, *Plasmodium* pKinI MD constructs do not form rings (Moores et al., 2006) and neither does *Drosophila* KLP59D (authors' unpublished data). Thus, our structural and sequence analyses provide an explanation for kinesin13s that form microtubule-associated rings and those that cannot.

There is considerable interest in proteins and protein complexes that encircle microtubules, because they may serve as molecular sleeves to keep cargoes attached to the end of dynamic microtubules (Salmon, 2005). The yeast kineto-chore DAM/DASH complex forms rings around microtubules in vitro, and it has been proposed that this complex mediates the attachment of kinetochores to dynamic microtubules in the mitotic spindle (Miranda et al., 2005; Westermann et al., 2005). We have speculated, on the basis of some common properties between kinesin13s and the DAM/DASH ring complex, that kinesin13s of higher eukaryotes may serve as a functional homolog of the DAM/DASH ring complex (Tan et al., 2006). However, it is still not clear whether protein complexes forming complete rings associate with microtubule ends in vivo (Davis and Wordeman, 2007). Electron tomography studies have not yet found any ring-like structures around microtubules in cells (Dong et al., 2007; McIntosh, 2005), but it is possible that they may not be well resolved or preserved by current techniques. Also, rings fully encircling the microtubule may not be required to keep

cargoes attached at the end of dynamic microtubules (Gestaut et al., 2008; Lombillo et al., 1995).

Perhaps the physiologically relevant structures are not rings fully encircling the microtubule but instead are smaller oligomers that utilize the same intermolecular contacts that mediate the formation of rings and spirals in vitro. In the case of kinesin13s, the presence of class-conserved residues, involved in the formation of microtubule-associated rings and spirals (Figure 5), suggests that these interactions are indeed important for kinesin13 function. Another possibility is that the oppositely oriented tubulin-binding sites on kinesin13 mediate interactions between adjacent microtubules in a kinetochore. Electrostatic interactions in the Kin-Tub-2 interface could bind the kinesin13 MD to a microtubule, while the Kin-Tub-1 site promotes pf peeling in an adjacent microtubule. Testing these and other possible physiological roles of the novel Kin-Tub-2 interface and kinesin13 ring-related oligomers requires further investigation. The ability to use site-directed mutagenesis to selectively disrupt the formation of rings from depolymerization activity, as shown here, will be an important tool to investigate the role of the kinesin13 ring structure in vivo.

EXPERIMENTAL PROCEDURES

Protein Constructs

Drosophila KLP10A MD construct includes residues I279 to I615 plus a 6His tag at the N terminus (Tan et al., 2006). Four mutant versions of this construct were prepared by replacing the following class-conserved residues: K317A, V318A, and D319A triple mutant (residues located in loop-2); K546A, E547A, and C548A triple mutant (residues located in α-helix-4); K350A (located in α-helix-1); and K399A (located in α-helix-2a). Mutations were introduced in the plasmid vector using the Quick-change site-directed mutagenesis kit (Stratagene). KLP10A MD constructs were expressed and purified as described elsewhere (Tan et al., 2006). Human KIF2A and KIF2C MD constructs contain residues S126–L526 of the HsKIF2A sequence and residues S226–G593 from the HsKIF2C. Both constructs have a 6His tag in the N-terminal ends. The human kinesin13 constructs (in the bacteria expression plasmid vector p28a-LIC) were a generous gift from the Structural Genomics Consortium, SGC (PDB ID: 2GRY and 2HEH). Bacterial expression and protein purification were performed as described in http://www.thesgc.com/sgc-webpages/StructureDescription.

Kinesin13 Microtubule Ring/Spiral Complex

Kinesin13 spiral complexes were prepared by incubating 1.5–3.75 μM polymerized tubulin and 1.5–7.5 μM kinesin13 MD constructs in BRB80 buffer (80 mM Pipes [pH 6.8], 2 mM $MgCl_2$, and 1 mM EGTA) supplemented with 2 mM $MgCl_2$, 2 mM AMP-PNP, and 20 μM taxol for 20 min at room temperature. The samples were spun (23,000× g for 10min at 28°C) to eliminate unbound proteins and were resuspended into 1/5 of the initial reaction volume before applying to grids to be flash-frozen for cryo-EM. Mixtures without spinning were used for negative stain EM experiments. When quantifying the ability to form rings of different kinesin13 constructs, an equimolar tubulin/kinesin13 ratio was used during incubation in all cases. Taxol-stabilized microtubules were prepared by polymerizing bovine

brain tubulin (Cytoskeleton) in BRB80 buffer supplemented with 5% DMSO and 20 μM taxol and 1 mM GTP, as described elsewhere (Desai and Walczak, 2001).

Negative Stain Electron Microscopy

Five microliters of the kinesin13-microtubule complexes was absorbed on freshly glow-discharged 400-mesh carbon coated grids for negative staining with 1% uranyl acetate. Images were taken with a FEI Tecnai T20 electron microscope at 120 kV and acquired with a 2K × 2K Tietz CCD camera (TVIPS, GmbH, Germany).

Immunogold Labeling

Antibody labeling was performed on grids containing already prepared kinesin13-microtubule complexes, as described above. Prepared grids were incubated with 10 μl of 40 μg/ml of a monoclonal antibody (TU-01, ab7750, AB-CAM) with epitope at the N-terminal of α-tubulin (residues 65–97) for 45 min at room temperature (in buffer A: BRB80 buffer plus 2mM Mg^{2+}-AMP-PNP, 20 μM taxol). Then the grids were rinsed five times with buffer A and incubated with10 μl of 20 μg/ml anti–mouse IgG conjugated with 10 nm colloidal gold (Electron Microscopy Science) for 45 min before negative staining.

Cryo-Electron Microscopy

Four microliters of the resuspension solution containing the KLP10A-microtubule complex (see above) were applied onto freshly glow-discharged holey-carbon grids (Quantifoil), blotted, and rapidly frozen using a Vitrobot apparatus (FEI). The grids were stored in liquid nitrogen before imaging. All images were recorded under low-dose conditions (<10 e/$Å^2$) in films at a nominal magnification of 50000 and nominal underfocus of 1–2 μm on either of two microscopes: FEI Tecnai T20 at an operating voltage of 120 kV or FEI Tecnai FEG F20 at an operating voltage of 200 kV.

Image Analysis

For 3D image reconstruction, we selected helical 15-pf microtubules from the images (Sosa and Milligan, 1996). Three-dimensional reconstruction was performed by the Fourier-Bessel algorithm (DeRosier and Moore, 1970) using routines from the software packages SUPRIM (Schroeter and Bretaudiere, 1996), MRC (Crowther et al., 1996), and PHOELIX (Carragher et al., 1996) and a suite of custom written Python scripts. Image defocus was estimated for each image by matching the zero positions on the power spectrum to calculated contrast transfer (CTF) functions. The defocus values in the final data set ranged from 1.5 to 2.5 μm. The CTF of each image was corrected by phase-flipping. An integral number of microtubule repeats were masked off and rein-terpolated to make the layer lines fall into integral pixels in the Fourier transform. Layer lines were extracted from several filament images and averaged after bringing them to a common phase origin. The final data set included 3296 asymmetric units. A 3D map was calculated from the averaged layer-line data-set by Fourier-Bessel inversion. The resolution of the map was estimated to be 2.8 nm by the Fourier Shell Correlation (FSC) 0.5 cutoff criteria (Frank, 2002)(Figure S1). Docking of the atomic structures of curved tubulin (PDB ID: 1sa0;(Ravelli et al., 2004), straight tubulin (PDB ID: 1jff;(Lowe et al., 2001), and kinesin13 MD (PDB ID: 1v8k;(Ogawa et al., 2004) with neck

residues not present in our KLP10A construct removed was done using the program COLORES from the SITUS software package (Chacon and Wriggers, 2002). The tubulin structures were fitted first independently into the 3D cryo-EM map. To fit the kinesin MD, the densities corresponding to the positioned tubulins were subtracted from the map. The tubulin densities to be subtracted were calculated from the atomic coordinates to the same resolution of the cryo-EM map using the program pdb2mrc from the EMAN package (Ludtke et al., 1999). Display of the 3D map and inspection of the docked of atomic structures was done with UCSF-Chimera (Pettersen et al., 2004).

Microtubule Depolymerization Assay

A turbidity assay was used to estimate the microtubule depolymerization activities of KLP10A MD constructs; 0.5 μM of KLP10A MD and 0.5 μM of taxol-MTs (in BRB80 buffer with 2 mM Mg^{2+}/ATP) were rapidly mixed in a spectrophotometer cuvette (Eppendorf UVette), and A350 was monitored for 20 min at 1 sec intervals in a PerkinElmer Lambda 25 UV/VIS spectrometer. Turbidity traces were converted to tubulin polymer concentration using a standard curve. The rate of tubulin polymer lost in the first 2 min of the reaction was plotted as the rate of depolymerization.

Supplementary Material

Refer to Web version on PubMed Central for supplementary material.

ACKNOWLEDGMENTS

We thank Hee-Won Park from the University of Toronto and Structural Genomics Consortium for the generous gift of DNA plasmids containing human kinesin13s KIF2A and KIF2C sequences; A. Asenjo for help with protein expression and discussions; D. Buster, D. Stokes, D. Sharp, and V. DePaoli for discussions and critical reading of the manuscript; and F. Macaluso, L. Gunther, and R. Diaz for help with electron microscopy. We gratefully acknowledge the facilities for electron microscopy at the Analytical Imaging Facility at AECOM and at the New York Structural Biology Center, which is a STAR center supported by the New York State Office of Science, Technology, and Academic Research. This project was supported by the National Institutes of Health (grant RO1-AR48620 to H.S.).

REFERENCES

Carragher B, Whittaker M, Milligan RA. Helical processing using PHOELIX. J. Struct. Biol. 1996; 116:107–112. [PubMed: 8742731]

Chacon P, Wriggers W. Multi-resolution contour-based fitting of macromolecular structures. J. Mol. Biol. 2002; 317:375–384. [PubMed: 11922671]

Crowther RA, Henderson R, Smith JM. MRC image processing programs. J. Struct. Biol. 1996; 116:9–16. [PubMed: 8742717]

Davis TN, Wordeman L. Rings, bracelets, sleeves, and chevrons: new structures of kinetochore proteins. Trends Cell Biol. 2007; 17:377–382. [PubMed: 17766118]

DeRosier DJ, Moore PB. Reconstruction of three-dimensional images from electron micrographs of structures with helical symmetry. J. Mol. Biol. 1970; 52:355–369. [PubMed: 5485914]

Desai A, Walczak CE. Assays for microtubule-destabilizing kinesins. Methods Mol. Biol. 2001; 164:109–121. [PubMed: 11217601]

Desai A, Verma S, Mitchison TJ, Walczak CE. Kin I kinesins are microtubule-destabilizing enzymes. Cell. 1999; 96:69–78. [PubMed: 9989498]

Dong Y, Vanden Beldt KJ, Meng X, Khodjakov A, McEwen BF. The outer plate in vertebrate kinetochores is a flexible network with multiple microtubule interactions. Nat. Cell Biol. 2007; 9:516–522. [PubMed: 17435749]

Frank J. Single-particle imaging of macromolecules by cryo-electron microscopy. Annu. Rev. Biophys. Biomol. Struct. 2002; 31:303–319. [PubMed: 11988472]

Ganem NJ, Compton DA. The KinI kinesin Kif2a is required for bipolar spindle assembly through a functional relationship with MCAK. J. Cell Biol. 2004; 166:473–478. [PubMed: 15302853]

Gestaut DR, Graczyk B, Cooper J, Widlund PO, Zelter A, Wordeman L, Asbury CL, Davis TN. Phosphoregulation and depolymerization-driven movement of the Dam1 complex do not require ring formation. Nat. Cell Biol. 2008; 10:407–414. [PubMed: 18364702]

Goldstein LSB, Philp AV. The road less traveled: emerging principles of kinesin motor utilization. Annu. Rev. Cell Dev. Biol. 1999; 15:141–183. [PubMed: 10611960]

Hirose K, Akimaru E, Akiba T, Endow SA, Amos LA. Large conformational changes in a kinesin motor catalyzed by interaction with micro-tubules. Mol. Cell. 2006; 23:913–923. [PubMed: 16973442]

Homma N, Takei Y, Tanaka Y, Nakata T, Terada S, Kikkawa M, Noda Y, Hirokawa N. Kinesin superfamily protein 2A (KIF2A) functions in suppression of collateral branch extension. Cell. 2003; 114:229–239. [PubMed: 12887924]

Ishikawa K, Kamohara Y, Tanaka F, Haraguchi N, Mimori K, Inoue H, Mori M. Mitotic centromere-associated kinesin is a novel marker for prognosis and lymph node metastasis in colorectal cancer. Br. J. Cancer. 2008; 98:1824–1829. [PubMed: 18506187]

Kikkawa M, Hirokawa N. High-resolution cryo-EM maps show the nucleotide binding pocket of KIF1A in open and closed conformations. EMBO J. 2006; 25:4187–4194. [PubMed: 16946706]

Lombillo VA, Stewart RJ, McIntosh JR. Minus-end-directed motion of kinesin-coated microspheres driven by microtubule depolymerization. Nature. 1995; 373:161–164. [PubMed: 7816099]

Lowe J, Li H, Downing KH, Nogales E. Refined structure of alpha beta-tubulin at 3.5 A resolution. J. Mol. Biol. 2001; 313:1045–1057. [PubMed: 11700061]

Ludtke SJ, Baldwin PR, Chiu W. EMAN: semiautomated software for high-resolution single-particle reconstructions. J. Struct. Biol. 1999; 128:82–97. [PubMed: 10600563]

Maney T, Wagenbach M, Wordeman L. Molecular dissection of the microtubule depolymerizing activity of mitotic centromere-associated kinesin. J. Biol. Chem. 2001; 276:34753–34758. [PubMed: 11466324]

Marx A, Muller J, Mandelkow EM, Hoenger A, Mandelkow E. Interaction of kinesin motors, microtubules, and MAPs. J. Muscle Res. Cell Motil. 2006; 27:125–137. [PubMed: 16362723]

McIntosh JR. Rings around kinetochore microtubules in yeast. Nat. Struct. Mol. Biol. 2005; 12:210–212. [PubMed: 15744320]

Mennella V, Rogers GC, Rogers SL, Buster DW, Vale RD, Sharp DJ. Functionally distinct kinesin-13 family members cooperate to regulate microtubule dynamics during interphase. Nat. Cell Biol. 2005; 7:235–245. [PubMed: 15723056]

Miranda JJ, De Wulf P, Sorger PK, Harrison SC. The yeast DASH complex forms closed rings on microtubules. Nat. Struct. Mol. Biol. 2005; 12:138–143. [PubMed: 15640796]

Moores CA, Yu M, Guo J, Beraud C, Sakowicz R, Milligan RA. A mechanism for microtubule depolymerization by KinI kinesins. Mol. Cell. 2002; 9:903–909. [PubMed: 11983180]

Moores CA, Cooper J, Wagenbach M, Ovechkina Y, Wordeman L, Milligan RA. The role of the kinesin-13 neck in microtubule depolymerization. Cell Cycle. 2006; 5:1812–1815. [PubMed: 16929184]

Ogawa T, Nitta R, Okada Y, Hirokawa N. A common mechanism for microtubule destabilizers-M type kinesins stabilize curling of the protofilament using the class-specific neck and loops. Cell. 2004; 116:591–602. [PubMed: 14980225]

Ovechkina Y, Wordeman L. Unconventional motoring: an overview of the Kin C and Kin I kinesins. Traffic. 2003; 4:367–375. [PubMed: 12753646]

Pettersen EF, Goddard TD, Huang CC, Couch GS, Greenblatt DM, Meng EC, Ferrin TE. UCSF Chimera–a visualization system for exploratory research and analysis. J. Comput. Chem. 2004; 25:1605–1612. [PubMed: 15264254]

Ravelli RB, Gigant B, Curmi PA, Jourdain I, Lachkar S, Sobel A, Knossow M. Insight into tubulin regulation from a complex with colchicine and a stathmin-like domain. Nature. 2004; 428:198–202. [PubMed: 15014504]

Rice LM, Montabana EA, Agard DA. The lattice as allosteric effector: structural studies of alphabeta- and gamma-tubulin clarify the role of GTP in microtubule assembly. Proc. Natl. Acad. Sci. USA. 2008; 105:5378–5383. [PubMed: 18388201]

Rogers GC, Rogers SL, Schwimmer TA, Ems-McClung SC, Walczak CE, Vale RD, Scholey JM, Sharp DJ. Two mitotic kinesins cooperate to drive sister chromatid separation during anaphase. Nature. 2004; 427:364–370. [PubMed: 14681690]

Salmon ED. Microtubules: a ring for the depolymerization motor. Curr. Biol. 2005; 15:R299–R302. [PubMed: 15854896]

Schroeter JP, Bretaudiere JP. SUPRIM: easily modified image processing software. J. Struct. Biol. 1996; 116:131–137. [PubMed: 8742734]

Shipley K, Hekmat-Nejad M, Turner J, Moores C, Anderson R, Milligan R, Sakowicz R, Fletterick R. Structure of a kinesin microtubule depolymerization machine. EMBO J. 2004; 23:1422–1432. [PubMed: 15029249]

Sindelar CV, Downing KH. The beginning of kinesin's force-generating cycle visualized at 9-A resolution. J. Cell Biol. 2007; 177:377–385. [PubMed: 17470637]

Sosa H, Milligan RA. Three-dimensional structure of ncd-decorated microtubules obtained by a back-projection method. J. Mol. Biol. 1996; 260:743–755. [PubMed: 8709152]

Sosa H, Dias DP, Hoenger A, Whittaker M, Wilson-Kubalek E, Sablin E, Fletterick RJ, Vale RD, Milligan RA. A model for the microtubule-Ncd motor protein complex obtained by cryo-electron microscopy and image analysis. Cell. 1997; 90:217–224. [PubMed: 9244296]

Tan D, Asenjo AB, Mennella V, Sharp DJ, Sosa H. Kinesin-13s form rings around microtubules. J. Cell Biol. 2006; 175:25–31. [PubMed: 17015621]

Westermann S, Avila-Sakar A, Wang HW, Niederstrasser H, Wong J, Drubin DG, Nogales E, Barnes G. Formation of a dynamic kinetochore- microtubule interface through assembly of the Dam1 ring complex. Mol. Cell. 2005; 17:277–290. [PubMed: 15664196]

Wordeman L. Microtubule-depolymerizing kinesins. Curr. Opin. Cell Biol. 2005; 17:82–88. [PubMed: 15661523]

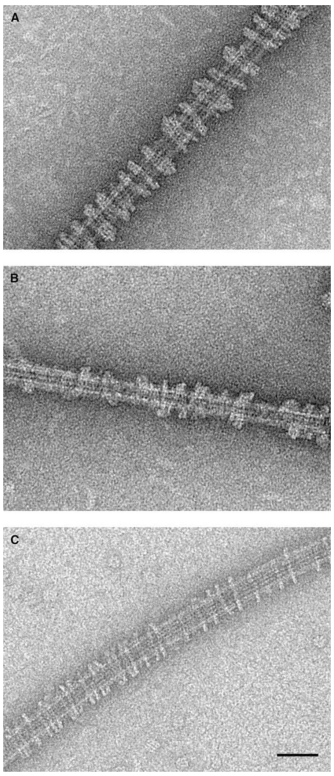

Figure 1. Human Kinesin13s KIF2A and KIF2C MD Form Rings Around Microtubules in the Presence of AMP-PNP

(A) *Homo sapiens* KIF2A

(B) *H. sapiens* KIF2C

(C) *D. melanogaster* KLP10A. Scale bar is 50 nm.

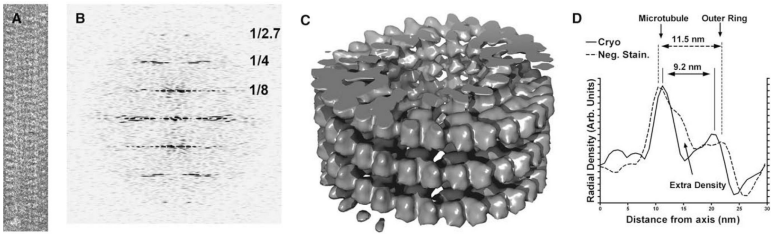

Figure 2. Cryo-EM 3D Reconstruction of KLP10A MD Spirals

(A) Cryo-electron micrograph of a 15-pf microtubule decorated with a KLP10A MD spiral.

(B) Power spectrum corresponding to image in panel a showing clear layer lines up to 1/2.7 nm^{-1} reciprocal spacing. Reciprocal spacings are indicated in the power spectrum in nm^{-1} units.

(C) Isosurface representation of a 3D map calculated from several cryo-EM micrographs of 15-pf microtubules decorated with KLP10A MD spirals.

(D) Comparison of the radial intensity profiles of a previous 3D reconstruction obtained from negative stained specimens (Tan et al., 2006) with the cryo-EM reconstruction showed in panel C.

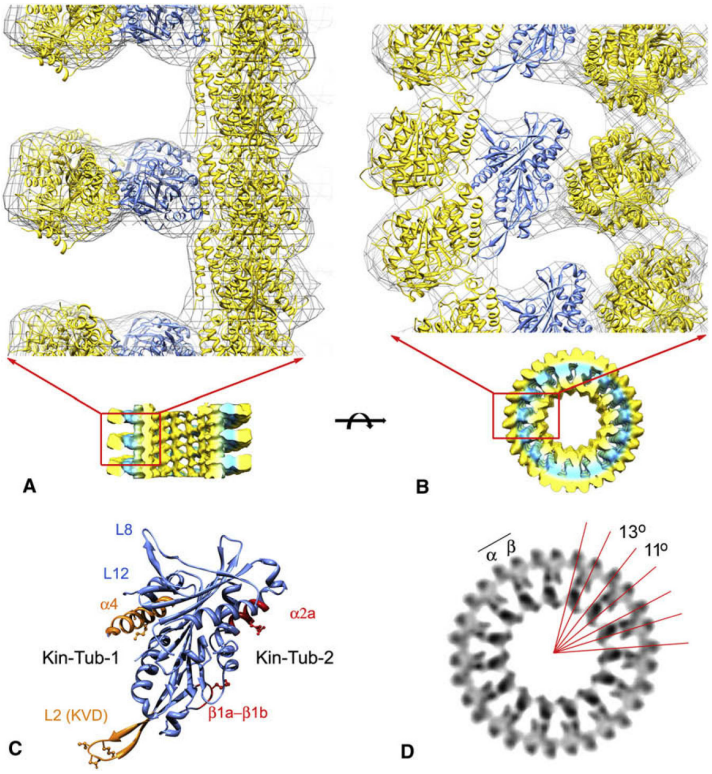

Figure 3. Molecular Model of the Kinesin13-Microtubule Ring/Spiral Complex

(A) Side view of the complex. The microtubule plus end is toward the top.

(B) End-on view of the complex from the microtubule plus-end. In panels A and B, the cryo-electron density map is represented as an isosurface gray cage enclosing the fitted atomic structures. The part of the map depicted in the top of the figure corresponds to the map shown in the bottom part. In panel a, the front of the microtubule is clipped away to show a side-view of the rings. The PDB identification codes of the fitted structures files are as follows: 1sa0 (Ravelli et al., 2004) for the curved tubulin in the outside ring, and 1v8k (Ogawa et al., 2004) kinesin13 MD and 1jff (Lowe et al., 2001) for the straight tubulin in microtubule. The fitted atomic models of tubulin and kinesin13 MD are shown in yellow and blue ribbon representations, respectively.

(C) Kinesin13 MD oriented as in panel b highlighting areas of interaction with tubulin.

(D) End-on volume projection of an 8 nm slice of the cryo-em map highlighting the radial angles between tubulin subunits.

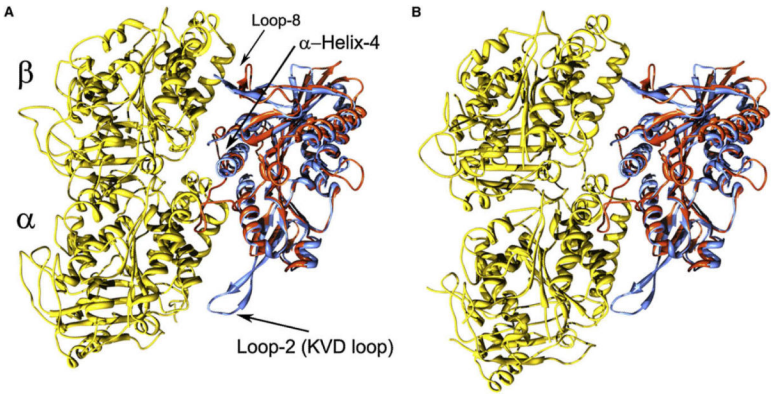

Figure 4. Comparison of Kinesin-Tubulin Complexes

For comparison, the kinesin13-curved tubulin complex and a recent kinesin1-microtubule complex model (PDB identification code 2p4n) (Sindelar and Downing, 2007) were superimposed by aligning conserved residues of the kinesin MDs.

(A) Yellow: straight tubulin heterodimer from the kinesin1-microtubule complex model. Red: kinesin1 MD. Blue: kinesin13 MD.

(B) Yellow: curved tubulin from the kinesin13-curved tubulin complex. Red: kinesin1 MD. Blue: kinesin13 MD. Regions α-helix-4 and Loop-2 containing the kinesin13 class specific sequences KEC and KVD are indicated.

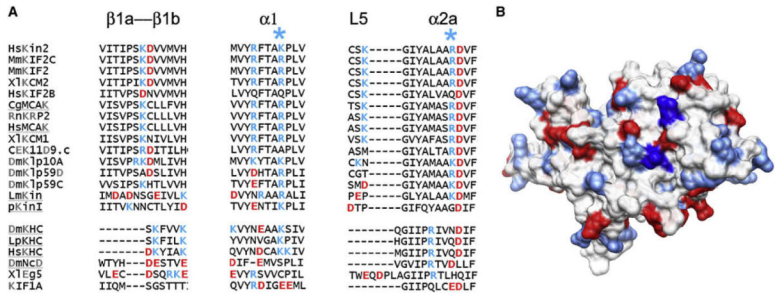

Figure 5. Kinesin13 Class-Conserved Residues Mediating Kin-Tub-2 Interactions

(A) Sequence alignments of regions of kinesin13 MD that are present at the Kin-Tub-2 interface. Kinesin13s are shown on top, and kinesins from other families are shown at the bottom. The * symbols highlight the columns corresponding to KLP10A residues K399 and K350.

(B) Surface representation of the kinesin13 MD(PDB ID 1v8k) (Ogawa et al., 2004) oriented to show the area forming the Kin-Tub-2 interface. Surface color coded according to amino acid charge (blue, positive; red, negative). The residues in the structure that after sequence alignment would correspond to KLP10A K399 and K350 are colored in dark blue.

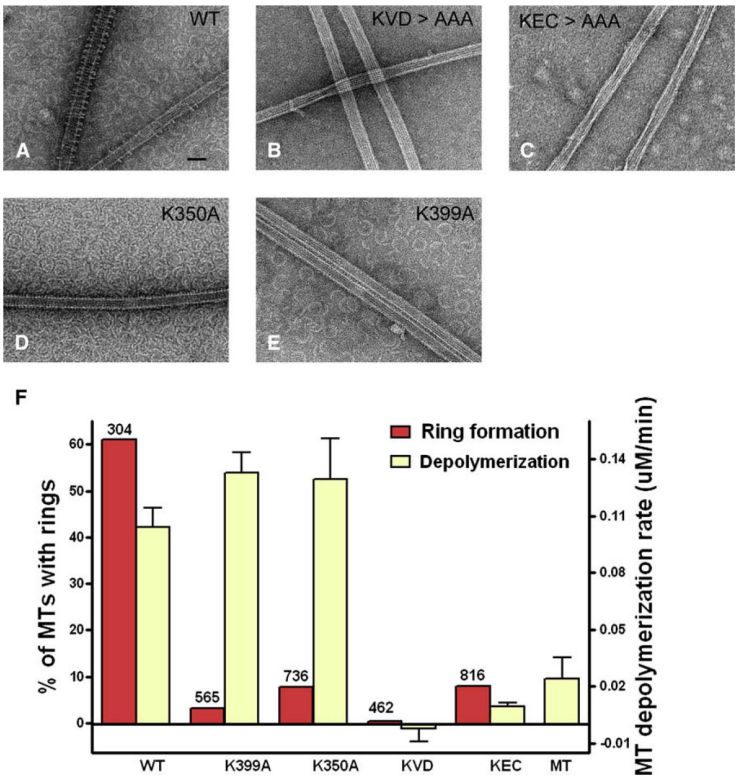

Figure 6. Site-Directed Mutagenesis of Residues Near Kinesin13-Tubulin Interaction Sites

(A–E) Negative stain electron micrographs of microtubules incubated with different KLP10A MD mutants.

(F) Ring formation (red bars, left *y* axis) and depolymerization activities (yellow bars, right *y* axis) of different KLP10A MD mutants. Bars for the depolymerization assays represent the means of the depolymerization rates, and error bars represent standard errors (n = 7 for all depolymerization assays). Ring formation activity was expressed as the percentage of microtubules that had at least one ring on them. The total number of microtubules inspected in each case is shown at the top of the bar.